

Journal of Materials Chemistry B

Accepted Manuscript



This is an *Accepted Manuscript*, which has been through the Royal Society of Chemistry peer review process and has been accepted for publication.

Accepted Manuscripts are published online shortly after acceptance, before technical editing, formatting and proof reading. Using this free service, authors can make their results available to the community, in citable form, before we publish the edited article. We will replace this *Accepted Manuscript* with the edited and formatted *Advance Article* as soon as it is available.

You can find more information about *Accepted Manuscripts* in the [Information for Authors](#).

Please note that technical editing may introduce minor changes to the text and/or graphics, which may alter content. The journal's standard [Terms & Conditions](#) and the [Ethical guidelines](#) still apply. In no event shall the Royal Society of Chemistry be held responsible for any errors or omissions in this *Accepted Manuscript* or any consequences arising from the use of any information it contains.



Journal Name

ARTICLE

Impact of phospholipids on plasmid packaging and toxicity of gemini nanoparticles

Chilbert Dong^a, Ildiko Badea^b, Masoomah Poorghorban^b, Ronald Verrall^c and Marianna Foldvari^{a*†}

Received 00th January 20xx,
Accepted 00th January 20xx

DOI: 10.1039/x0xx00000x

www.rsc.org/

Understanding the relationship of structural modifications on the assembly and disassembly of synthetic or non-viral gene delivery is crucial with regard to their rational development. This study describes the use of fluorescence correlation spectroscopy (FCS), as a new tool, to investigate the effect of systematic chemical modifications to dicationic N,N-bis(dimethylalkyl)- α,ω -alkanediammonium surfactants (gemini surfactants) on the self-assembly and physical properties of a series of gemini nanoparticles (gemini NPs). A systematic screening of 27 gemini-plasmid (GP) complexes and gemini NPs showed that their final morphology is governed by the pre-compactation of plasmid by the gemini surfactants. The assembly process of gemini-plasmid intermediate complex (GP) and the final gemini NP (or gemini-plasmid-lipid complex, GPL) was monitored by the tracking of the Cy5-labeled plasmid. Based on diffusion properties, GP complexes were larger than gemini NPs (300-500 nm for GP and 200-300 nm for GPLs). Stoichiometric analysis of the raw intensity histograms showed that both GPs and GPLs particles were composed of multiple plasmids. The final GPLs contain fewer plasmids (2-20 per particle) compared to the intermediate GP (5-35 per particle). The addition of phospholipids dispersed and stabilized GPs to form GPL, but the type of phospholipid (DOPE or DD 1:3) had little effect on the final size of the particles. The FCS data were both validated and complemented by the results of studies of dynamic light scattering (DLS), atomic force microscopy (AFM), X-ray scattering and dye-exclusion assays. A model for gemini NP assembly involving supramolecular aggregate intermediates is proposed.

Introduction

Nanomedicine, the application of nanotechnology towards diagnosis, monitoring and treatment, has rapidly gained interest because of its potential to revolutionize health care including gene therapy^{1, 2}. Nanotechnology offers new methods to deliver biological macromolecules using non-viral gene carriers to overcome barriers to improve these therapies. Non-viral gene carriers are safer alternatives to viral vectors, but suffer from low efficacy.³

Previously we have shown that a new class of non-viral gene carriers, gemini nanoparticles (NPs), facilitate gene delivery both *in vitro* and *in vivo*.⁴⁻⁷ Gemini NPs are composed of dicationic gemini surfactants (N,N-bis(dimethylalkyl)- α,ω -alkanediammonium surfactants, having two cationic head groups and two alkyl tails with the general structure $[C_mH_{2m+1}(CH_3)_2N^+(CH_2)_sN^+(CH_3)_2C_mH_{2m+1}.2X^-]$; abbreviated as m-s-m, where m and s refer to the number of carbon atoms in the alkyl tails and in the polymethylene spacer group, respectively; and X is the counter ion). They have unique physical properties that make them suitable candidates as building blocks for non-viral gene carriers.⁸⁻¹⁰ Several studies have also shown that the effectiveness of the gemini NPs can be tuned through chemical modifications to the basic gemini surfactant structure. The results have

^a School of Pharmacy and Waterloo Institute of Nanotechnology and *The Centre for Bioengineering & Biotechnology University of Waterloo, Waterloo, ON, Canada N2L 3G1

^b College of Pharmacy and Nutrition University of Saskatchewan, Saskatoon, SK, Canada S7N 2Z4

^c Department of Chemistry, University of Saskatchewan, Saskatoon, SK, Canada S7N 5C9

[†] Corresponding author: M. Foldvari, D.Pharm. Sci., PhD foldvari@uwaterloo.ca

shown that short spacers and longer tails correlate with higher transfection efficiency⁹. Substitutions such as the addition of various chemical groups have been shown to add important functionality to the gemini NPs, such as response to pH and increased biocompatibility^{4, 11}

While a wide variety of techniques have been employed to study non-viral gene carriers in great detail, nanoparticle assembly in real time and in the context of the biological environment is relatively poorly understood.¹²⁻¹⁵ To advance the field of non-viral gene delivery towards *in vivo* applications, more information is required on the effects of NP composition and structure on gene delivery capabilities. A new characterization technique, fluorescence correlation spectroscopy (FCS), can provide direct information about the interaction and dynamics of molecules within the nanoparticles. FCS utilizes high spatial and temporal analysis to measure the minute fluctuation in fluorescence intensity in a small population of molecules at equilibrium. From these fluctuation patterns, one can extract various biophysical properties of the molecules. Fluctuations can occur over a wide variety of time ranges and include shifts in molecular orientation (picoseconds), blinking or triplet state transitions (microseconds) and molecular interactions such as binding and chemical reactions (milliseconds).^{16, 17} Previously used mainly in biology, FCS, is now finding applications in a wide variety of fields including material sciences and drug delivery.¹⁸⁻²⁰

In this study we applied FCS to probe the assembly of gemini NPs and used an additional extension of FCS, intensity histogram analysis, as a simple and effective tool to directly monitor the amount of plasmid within a non-viral gene carrier (Figure 1, i). We have extended the FCS methodology to study the biophysical properties

of gemini NPs and to evaluate the effects of the chemical structure of a series of gemini surfactant components on the stoichiometry of the final complex (Fig 1, ii). Using additional methods such as dynamic light scattering, zeta potential measurements, atomic force microscopy and small-angle x-ray scattering (SAXS), a full physicochemical profile of the NPs was obtained and a model for NP assembly was developed. FCS application to NP characterization introduces a powerful analytical tool to study the assembly of gemini NPs in a wide variety of environments in real-time and provides a better understanding of the biophysical properties of NPs so as to advance the rational development of non-viral gene delivery systems and improve efficiency, effectiveness and safety.

Materials and Methods

NP components

Plasmid DNA (gWiz GFP; 5757 bps) was purchased from Aldevron (Fargo, ND, USA). Plasmids were routinely checked for purity and topology using spectroscopy and agarose gel electrophoresis, respectively. A series of gemini surfactants listed in Table 1 were previously synthesized as described elsewhere^{21, 38, 39}. The gemini surfactants in this study were systematically selected to investigate change to carbon spacer and tail length and functionalization. Gemini surfactant solutions were prepared at 3mM with milli-Q grade water. Aliquots were stored at 4°C and used immediately after warming to room temperature. DOPE (1,2-di-(9Z-octadecenoyl)-sn-glycero-3-phosphoethanolamine) and DPPC (1,2-dihexadecanoyl-sn-glycero-3-phosphocholine) were obtained from Avanti Polar Lipids (Alabaster, AL, USA).

Nucleic acid labeling

The plasmid gWiz GFP was labeled with Cyanine 5 fluorophore (Cy5) using the Cy5 LabelIT® Tracker kit from Mirus Bio LLC (Madison, WI, USA) at 0.25:1 (w/v) labeling reagent-DNA ratio. Labeling gWiz GFP (Cy5-gWiz) was purified by ethanol precipitation and filtration through Amicon Ultra centrifuge filters (3kD cutoff) from Millipore Corporation (Billerica, MA, USA). Labeling density was determined from the ratio of base to dye using the equation:

$$\text{Base:Dye} = \frac{(A_{\text{nucleic acid}} \times \epsilon_{\text{Cy5}})}{(A_{\text{Cy5}} \times \epsilon_{\text{nucleic acid}})} \quad (\text{Eq. 1})$$

where $A_{\text{nucleic acid}}$ and A_{Cy5} are the absorbances measured at 260 nm and 649 nm, respectively. The values of the extinction coefficients for nucleic acid and Cy5 dye were previously determined to be $\epsilon_{\text{Cy5}} = 250,000$; $\epsilon_{\text{nucleic acid}} = 6,600$, respectively. A correction factor ($\text{CF}_{260} = 0.05$) was added to the $A_{\text{nucleic acid}}$ measurement using the equation $A_{\text{nucleic acid}} = A_{260} - (A_{\text{Cy5}} \times \text{CF}_{260})$. The raw intensity data were plotted as a histogram to show the distribution of the photon intensity. It showed that Cy5-gWiz GFP had an average intensity of 250 kHz, with the majority of the peaks occurring between 150-300 kHz, and a long tail resulting from a small number of measurements ranging up to 5000 kHz. This variation in peak intensity is indicative of different degrees of labeling, or the presence of small populations of aggregates. To ensure this was not an artifact due to the presence of free dye or dye aggregates, additional purification steps by ethanol precipitation and centrifugation were performed. This additional purification did not remove the larger signal peaks and resulted in the decrease of the diffusion

coefficient due to increased DNA degradation (data not shown). Furthermore, the agarose gel did not reveal the production of a significant amount of aggregation in the plasmid DNA due to the labeling process. Overall, the presence of the brighter peaks in the Cy5-gWiz GFP did not interfere with the quality of the FCS measurement and confirmed that the only source of fluorescence was due to the presence of the labeled plasmids. The degree of labeling was calculated to be approximately 10 per plasmid. The Cy5-gWIZ was characterized at a concentration of 2 ng/ μL experimentally determined to be optimal for FCS measurements, corresponding to a mean particle number (N) of 1.

Confirmation of super-coiled plasmid and purity

Purity of unlabeled and labeled gWiz GFP was determined by measuring the absorbance at 260 and 280 nm, respectively, using a Nanodrop 2000C spectrophotometer (Thermo Scientific, Wilmington, DE, USA). The topology of Cy5-plasmid was determined by electrophoresis on a 0.8% agarose gel run at 80V for two hours. Supercoiled DNA was quantified using densitometric analysis with ImageJ software (National Institutes of Health, Maryland, USA).

Liposome component preparation

Liposomes (neutral helper lipids) composed of either pure DOPE or DOPE and DPPC at a ratio of 0.25:0.75 (DD 1:3) were prepared by the thin-film method. Lipids were dissolved in 100% ethanol in a round bottom flask. Thin-films were deposited by removal of solvent with a rotary evaporator under vacuum at 50°C at 150 rpm. Trace amounts of solvent were removed by freeze-drying (Labconco) for 4 hours. The lipid thin-film was re-hydrated to a concentration of 3mM with a 9.25% w/v sucrose solution (pH 7) at 50°C for 30 minutes

to produce crude/multi-lamellar liposomes. Crude liposome solutions were sonicated for 30 minutes in a bath sonicator (VWR 75D, VWR International LLC, PA, USA) until translucent. Liposomes were filtered through a 0.45 μm cellulose filter prior to use. Liposome size was routinely checked by DLS using a Zetasizer Nano ZS (Malvern Instruments Ltd, Worcestershire, UK) and determined to be approximately 150 nm.

Gemini nanoparticle preparation

Gemini NPs were prepared in a two-step process. Primary assembly consisted of the addition of gemini surfactant to 0.5 μg of Cy5-plasmid to obtain a charge ratio ($\rho_{+/-}$) of 10:1 and incubated at room temperature for 15 minutes to form the gemini-plasmid DNA (GP) complex. The second assembly step requires the addition of 75 μL of 1mM DOPE or DOPE:DPPC liposome to GP and further incubation for an additional 30 minutes to form GPL or gemini NP.

Fluorescence correlation spectroscopy experimental set-up

FCS measurements were performed on a commercial Zeiss LSM 710 microscope with Confocor 3 system (Zeiss, Jena, DE). Cy5 was excited by a 633 nm He-Ne laser at approximately 50 μW and reflected by a dichroic beam splitter (488/633) and focused 200 μm into the sample through a 40x Zeiss Apochromat NA 1.2 water-immersion objective lens. Emission spectra were collected through a 580 nm long-pass filter and recorded by an avalanche photo-detector (APD). Out-of-focus emission was blocked by a pair of confocal pinholes set at 45 μm. The lateral radius of the focal volume for the 633 nm laser was determined by a calibration dye (Cy5-NHS-ester) to be 250 nm. FCS measurements were carried out in 200 μL volumes of diluted gemini NP

in a 4-well CELLview coverslips (Grenier-Bio One, Frickenhausen, DE). NP samples were prepared in triplicate for FCS and measurements taken for 10 s, twenty-five times for each sample. Calibration of the system was performed with a 50 nM Cy5 solution. Using the known diffusion coefficient of rhodamine G6 ($3.2 \times 10^{-10} \text{ m}^2 \text{ s}^{-1}$), the lateral (ω_R) and axial (ω_z) radii of the focal volume was determined to be respectively of 0.25 and 1.6 μm, giving a focal volume of 0.19 fL using the equation below ((Eq. 2)

$$V = \frac{\pi^{3/2}}{2} \omega_R^2 \omega_z \quad (\text{Eq. 2})$$

FCS data analysis

The autocorrelation function (ACF) was determined from the count rate collected from the APD as described elsewhere⁴⁰. Assuming a three-dimensional Gaussian excitation intensity distribution, the free diffusion of a single species was calculated using the formula:

$$G(t) = \frac{1}{N} \left(1 + \frac{\tau}{\tau_d}\right)^{-1} \left(1 + \frac{\tau}{S^2 \tau_d}\right)^{-1/2} \quad (\text{Eq. 3})$$

where N is the mean number of molecules in the excitation volume, S is the ratio between the equatorial and axial radii of the focal volume, and τ_d is defined as the characteristic diffusion time of the particle. Diffusion coefficients (D) were determined using the Stokes-Einstein equation shown below.

$$D = \frac{\omega_R^2}{4\tau_d} \quad (\text{Eq. 4})$$

where ω_R is the lateral radius of focal volume experimentally determined by measuring the

diffusion time of calibration dye ($\tau_{d,Cy5}$) with a known diffusion coefficient (Cy5 NHS-ester; $D_{Cy5}=3.2 \times 10^{-6} \text{ cm}^2/\text{s}$). τ_d for the sample is obtained from the fitted ACF. FCS data was analyzed using Confocor 3 Software Zen 2009 (Jena, DE). Files were exported into Origin 7.5 (Microcal, MA, USA) to plot ACF and intensity histograms. All reported diffusion coefficients were averaged based on at least 4 individual measurements.

Particle size and zeta potential measurements

Particle size and zeta potential measurements were performed simultaneously using the Zetasizer Nano (Malvern Instruments Ltd, Worcestershire, UK). Particle size was determined using DLS and zeta potential was determined using laser Doppler micro-electrophoresis (LDME). Gemini NPs were prepared at a $\rho_{+/-}$ 10:1 as described previously. Measurements were carried out with 70 μL of aqueous solution in micro-cuvette (Brandtech Scientific, CT, USA). Samples were prepared in triplicates and four aliquots were measured five times for DLS and LDME. pH of all formulations were determined using a Twin compact pH meter (Horiba Scientific, Kyoto, JP). pH of GPs and GPLs were between 6.5-7.1.

Atomic force microscopy

AFM measurements were performed on a PicoSPM instrument (Molecular Imaging, Tempe, AZ) operating in MAC mode[®] using an AFMS or AFMM scanner. Type II MACLever cantilevers (Molecular Imaging, Tempe, AZ) with spring constants in the range of 1.2-5.5 N/m, or MSC12 silicon cantilevers (Mikromasch, Portland, OR) with spring constants in the range of 0.15-1.5 N/m, were used for MAC mode imaging. All measurements were performed at ambient conditions with the instrument mounted in a vibration isolation system. The scanning speed was

1-2 lines per second. Freshly cleaved Grade V-4 mica (SPI Supplies) was used as a substrate for all AFM measurements.

Transmission electron microscopy

Electron microscopy was carried out by negative staining of NPs with 1% (w/v) phosphotungstic acid on carbon coated 200 mesh copper grids, and images were taken by a JEOL 2010F field-emission transmission electron microscope at the Canadian Centre for Electron Microscopy at McMaster University (Ontario, Canada). The accelerating voltage was 80 kV.

Small-angle x-ray scattering

SAXS measurements were performed at the BL4-2 beamline at Stanford Synchrotron Radiation Lightsource (SSRL, Stanford, USA) at a energy of 11 keV and a sample to detector distance of 1.1 m at 20-30 s exposure time. Diffraction intensity versus q plots were obtained by radial integration of the 2D patterns using GSAS II.

Dye exclusion assay

Gemini NPs were prepared at a $\rho_{+/-}$ 10:1 as described previously. For PicoGreen dye exclusion assay, NPs were diluted 10-fold in water and incubated with PicoGreen dye prepared as recommended by the manufacturer for 5 minutes prior to measurement. NPs were diluted 5-fold in water for EtBr assay and incubated with EtBr dye (Bio-Rad Laboratories Ltd., Hercules, CA, USA) prepared at a final concentration of 1 $\mu\text{g}/\text{mL}$ for 5 minutes. Fluorescence measurements were made on the Spectramax M5 spectrophotometer at 485 nm and 560 nm for PicoGreen and 250 nm and 605 nm for EtBr⁴¹. To assess the quantity of DNA, a standard curve was prepared from gWiz plasmid for both PicoGreen and EtBr dye exclusion assays

to determine the amount of detectable DNA in NPs.

Cell culture and PrestoBlue viability assay

The origin and characterization of the parental PAM 212 cells has been described previously⁴². The PAM 212 cell line is a spontaneously malignant transformed cell line derived from neonatal BALB/c keratinocytes *in vitro*, and was provided by Dr. Stuart Yuspa of the National Cancer Institute. The PAM 212 cells were cultured using MEM plus media with 10% FCS and 1% penicillin and streptomycin. The cells were routinely cultured at 37°C in a 5% CO₂ and humidified atmosphere until ~70-80% confluency. PAM 212 cells were seeded at 20,000 cells per well in black clear-bottom 96-well plates and incubated for 24 hours. At 80% confluency, cells were washed with MEM and treated with Lipofectamine or gemini GPs and GPLs in quadruplicate for five hours followed by removal of NPs and incubation for 24 hours in supplemented MEM. Cells were washed and incubated with 10 µL of PrestoBlue® (Invitrogen, CA, USA) per well in 90 µL of basic MEM for 10 minutes at 37°C. PrestoBlue was excited at 535 nm and emission was measured at 615 nm using a spectrophotometer (Spectramax M5, Molecular Devices, CA, USA).

Statistics

Statistical analysis was performed using SPSS V 17.0. For FCS data sets, data was transformed to a log basis to account for non-normality prior to two-way ANOVA analysis. One-way ANOVA was used to determine the significance for particle size, zeta potential and transfection studies. Significance was determined between experimental groups with a $p < 0.05$ level.

Results

Preparation of the labelled plasmid for FCS

Gemini NPs are formed by a two-step process; the first step is the pre-compaction of plasmids with cationic gemini surfactant molecules to form the gemini-plasmid complex (GP) followed by the spontaneous self-assembly of gemini NPs by the addition of neutral phospholipids (GPL) (Figure 1, iii). The assembly process was monitored by tracking the fluorescently labeled gWIZ model plasmid. The Cy5 labeling of the plasmid was carried out at 0.05:1, 0.25:1 and 0.5:1 mol ratios and the most optimal labeling was achieved at 0.05:1 and 0.25:1 labeling ratios with low variation in diffusion coefficients ($D_{0.05} = 3.6 \pm 0.3 \times 10^{-12} \text{ m}^2/\text{s}$ and $D_{0.25} = 4.2 \pm 0.2 \times 10^{-12} \text{ m}^2/\text{s}$, $n=4$) and high preservation of the supercoiled form of the plasmid. At the 0.5:1 labeling ratio, a large portion of the plasmid (at least 40%) was nicked into an open circular form resulting in a shift in the diffusion coefficient ($D_{0.5} = 7.1 \pm 0.7 \times 10^{-12} \text{ m}^2/\text{s}$). The reproducibility and yield was highest with the 0.25:1 labeling ratio, hence these conditions were used to prepare the Cy5-labeled plasmid for the FCS experiments. The autocorrelation curves for Cy5-plasmid (Figure 2 i, A and D) were satisfactorily fitted using a one-component free diffusion model described in Eq. 3. The plasmid concentration was normalized for all samples at 2 ng/µL so that any shifts in the FCS profiles of plasmid were due to interactions with other components during NP assembly.

By evaluating the intensity histograms of the free plasmid, GP and GPL and comparing the changes that occur one can gain insight into the distribution of plasmids within the NP population. Figure 2 i, A shows the raw photon stream from the avalanche photo-detector (APD) for the free Cy5-plasmid. This plot shows that although the

count rates fluctuate, randomly, they equilibrate around an average value or baseline of approximately 240 kHz. Since the concentration of free Cy5-plasmid was determined to be approximately 1, it suggests that on average most plasmids passing through the focal volume have an intensity of approximately 240 kHz. Some of the fluorescent fluctuations are more intense than others due to the uneven labeling of plasmid. This resulted in small spikes in intensity, but was shown not to affect analysis since the autocorrelation function could be calculated and fitted. To gain a better understanding of the distribution of peak intensities, the data were re-plotted in the form of a histogram (Figure 2 i, D). The Cy5-plasmid generally has a bell-shaped distribution with a significantly long tail on the right-side of the maxima. The larger spikes represent a small population of brighter molecules within the population of plasmids which could be due to uneven labeling or the overlap of fluorophores in the focal volume; however, these events were rare and had little impact on the calculation of the autocorrelation function. Since all samples in the FCS study contained the same amount of Cy5-plasmid, any changes in the characteristics of the intensity histogram profile can be related to the addition of the gemini surfactant and neutral phospholipids.

FCS analysis of gemini NP assembly

The gemini surfactants in this study were selected to systematically evaluate three key modifications: spacer (12-s-12; s=3,6,7,10 and 16), tail (m-3-m; m=12,16 and 18) and addition of functional group (Py-3-12 and 12-7NH-12), based on studies performed previously by our group^{4, 9, 21}. GPs were prepared with Cy5-plasmid and unlabeled gemini surfactants at a ($\rho_{+/-}$: 10:1). Raw intensity count rates and intensity histograms

were obtained for all plasmid, GP and GPL particles. Representative graphs are shown in Figure 2, i, B, E and C, F.

The GP complexes represent a fairly heterogeneous population of large particles. The autocorrelation curve of Cy5-plasmid after the addition of gemini surfactant 12-3-12 (GP complex) demonstrated two major shifts compared to the autocorrelation curve of free Cy5-plasmid (Figure 2, ii). The first is a significant upward translation of the curve. This number corresponds to the inverse of the $G(\tau)$ which represents a decrease in the mean number of molecules as a result of a decrease in the number of individual fluorophores in solution passing through the focal volume. The second change is a horizontal translation of the curve to the right. To emphasize the shift in diffusion time between free Cy5-plasmid and GP the mean number was normalized to 1. The diffusion coefficient of the 12-3-12 GP complexes was $0.98 \pm 0.31 \times 10^{-12} \text{ m}^2/\text{s}$ (n=4) and their diameter, calculated using the Stokes-Einstein equation (Eq. 4), was estimated to be 502.2 nm (CV 31.66 %) which is in good agreement with DLS and AFM results (Table 1 A and Figure 4). The diffusion coefficients of all GPs formed from the gemini surfactant series are shown in Table 1. In the series of gemini surfactants used to form GP complexes, FCS results showed that changes in spacer length resulted in a non-linear shift in the diffusion coefficient of GPs (Figure 2, iii, Panel I). The diffusion coefficient for GPs was highest for s=10 ($4.15 \times 10^{-12} \text{ m}^2/\text{s}$) and decreased as spacer length became shorter or longer. Similarly, increasing carbon tail length also resulted in an increase in diffusion coefficient when comparing 12-3-12 to 16-3-16 (0.98 vs $1.91 \times 10^{-12} \text{ m}^2/\text{s}$, respectively). This trend could not be extended onto 18-3-18 due to issue with aggregation caused by very low CMC²².

The most significant change was observed with the introduction of functional groups. Both Py-3-12 and 12-7NH-12 formed smaller GPs compared to their parent gemini surfactant (12-3-12 and 12-7-12, respectively) (Figure 2, iii, Panel I C).

GPLs caused shifts to the autocorrelation curves. Compared to GPs, the GPLs show both a downward and shift to the right of the curves (Figure 2, iii, Panel II). This indicates an increase in the number of particles and that the particles also move faster through the focal volume ($D_{\text{GPL-12-3-12}}=3.1\pm 0.4 \times 10^{-12}$ (n=4), $D_{\text{GP-12-3-12}}=1.0\times 10^{-12} \pm 0.3$ (n=4)). The model described by Eq. 3 when fitted to the autocorrelation curves showed a tighter fit for GPLs compared to the GPs.

Overall, the magnitude of the diffusion coefficient of most GPLs was between $3.2\text{-}3.3\times 10^{-12}$ m²/s. As a result, the calculated particle sizes for the majority of GPLs were also quite uniform with an average of approximately 120 ± 30 nm. This uniformity is also reflected in the autocorrelation function (ACF) of the phospholipids. In contrast to the GP complexes, which were composed of large and heterogeneous particles of approximately 300-500 nm, the addition of phospholipid normalized the size and produced smaller and more uniform NPs (120-150 nm).

Estimation of the number of plasmids within gemini NP

Characterization techniques such as DLS, AFM and TEM can study the external morphology and size of the NPs but cannot confirm if the particles in fact contain DNA or even the approximate quantity, whereas FCS can monitor both the size and internal composition of nanoparticles. By evaluating the intensity histograms of the free plasmid, GP and GPL the number of plasmids within the particles was

estimated. The GPs were large particles composed of a large number of plasmids (Figure 2 i, B, E) evident from the significant upward shifts in the intensity histogram profile of the Cy5-plasmid upon the addition of gemini surfactants. The intensity histogram revealed a very long tail to the right and showed a major increase in the brightness of the GP compared to free cy5-plasmid. Since the focal volume is restricted, these labeled plasmids are concentrated within very close proximity (<250 nm) to cause these large spikes in intensity. Since previously it was established that each plasmid has an average brightness of 240 kHz, the larger peaks with intensities of 10,000 kHz, are estimated to contain over 40 plasmids. Figure 2 iv illustrates the distribution of the number of plasmids per particle in GP and GPL particles prepared with three different gemini surfactants. The average number of plasmids per particle, estimated based on average individual counts per particle (kHz) divided by average individual counts of plasmid (240 kHz), was 10.6 ± 9.3 (12-3-12GP), 9.9 ± 6.4 (py-3-12GP) and 8.0 ± 5.6 (12-7NH-12GP) (Figure 2 iv). The intensity study also revealed that the addition of the gemini surfactants effectively complexed all the plasmids in solution indicated by the loss of the previous maxima (240 kHz for Cy5-plasmid) and a shift of the maxima to between 0-50 kHz (background levels). The addition of phospholipids resulted in the formation of more homogeneous GPL particles compared to the GP complexes (Figure 2 i, G and F) and the number of particles per unit volume was also greater as seen from the increase in the number of peaks. The average number of plasmids per particle in GPL was 7.8 ± 5.1 , (12-3-12GPL_{DOPE}), 8.0 ± 5.5 (py-3-12GPL_{DOPE}) and 10.3 ± 9.7 (12-7NH-12GPL_{DOPE}); and 9.0 ± 7.6 , (12-3-12GPL_{DD}), 3.2 ± 4.3 (py-3-12GPL_{DD}) and 7.3 ± 6.9 (12-7NH-12GPL_{DD}) (Figure 2 iv).

Particle size and zeta potential by Zetasizer

To validate FCS as a tool to monitor physiochemical parameters of GPLs, key physical characteristics of GPLs such as particle size and zeta potential were measured using Zetasizer for various compositions at various stages of assembly. Size distribution of Cy5-plasmid, was heterogeneous, $300 \text{ nm} \pm 400 \text{ nm}$, with a high PDI of 0.5 ± 0.3 ($n=4$), simply showing that free plasmid alone is not compacted and the measurement is of low reliability based on the DLS correlogram. Phospholipid vesicles prepared with DOPE or DD 1:3 by thin-film method had a final average diameter of $120 \pm 30 \text{ nm}$ and $140 \pm 20 \text{ nm}$ ($n=4$) and narrow size distribution with PDI of 0.2 and 0.23, respectively. GPLs in general had diameters in the range of 100-200 nm (Figure 3 A, B; Table 1 B). Overall, the type of phospholipids used to prepared the GPL resulted in a small change in size ($Z\text{-Avg}_{\text{GPLDD1:3}}=159 \pm 47 \text{ nm}$ and $Z\text{-Avg}_{\text{GPLDOPE}}=168 \pm 42 \text{ nm}$), but statistically insignificant between the two groups. The only exception to this trend was with the imine gemini surfactant (12-7NH-12) where the DD 1:3 GPL was significantly larger than the GPL prepared with DOPE. Within each group of GPLs, trends arose once again based on the gemini surfactant used to compact the plasmid. For $m=12$ the gemini spacer length shows a trend of decreasing size starting from the 3C spacer ($206 \pm 8 \text{ nm}$) down to a minimum for the 7C spacer ($115 \pm 24 \text{ nm}$) with an increase in particle size up to 12-16-12 ($178 \pm 15 \text{ nm}$). Similarly, an increase in the carbon tail length of the gemini surfactants, e.g., for $m=12$ to 16 and $s=3$ resulted in a decrease of particle size ($172 \pm 40 \text{ nm}$), but this trend could not be extended to 18-3-18 due to aggregation in the sample. The addition of functional groups to the spacer or tail region of the gemini surfactants in the form of the 12-7NH-12 and Py-3-12 also resulted in smaller size GPLs ($123 \pm 35 \text{ nm}$ and $125 \pm 28 \text{ nm}$,

respectively), suggesting that gemini surfactants do not only aid in the production of smaller, but also more uniform particles depending on specific structural modifications. Furthermore GPLs prepared from DD1:3 were smaller in size but showed a larger PDI compared to their DOPE counterparts due to the mixing of different lipids resulting in greater heterogeneity of GPLs^{23, 24}. Compared to GPs that had a broad size distribution and larger particle sizes ($\text{PDI}_{\text{avg}}=0.38$, 450 nm), the addition of neutral phospholipids created a more homogenous population of smaller particles ($\text{PDI}_{\text{avg}}=0.28$, 150 nm) (Figure 3 A).

All gemini surfactants in this study were able to effectively neutralize the negative charge of the plasmid (-63 mV). Zeta potential data showed that all GPs carried a low to moderate positive charge (from close to 0 mV to $+20 \text{ mV}$) (Figure 3 C, D). Beyond neutralizing the plasmids, it was shown that the structure of the gemini surfactants also governed the final charge of the GPs. An increase in the carbon chain length of either the spacer or the tail region of the gemini surfactant resulted in a significant increase in zeta potential. However, modifications to the tail regions resulted in greater changes compared to the spacers ($\delta_{18-3-18}=+44 \text{ mV}$, $\delta_{12-10-12}=+20 \text{ mV}$). The introduction of functional groups was also shown to have a significant effect on the surface charge. GP complexes made either with 12-7NH-12 ($9.6 \pm 2 \text{ mV}$) or Py-3-12 ($24.64 \pm 2.8 \text{ mV}$), had significantly higher surface charge compared to their parent compounds ($\delta_{12-7-12}=6.71 \pm 0.4 \text{ mV}$ and $\delta_{12-3-12}=0.09 \pm 0.4$, respectively).

Regardless of gemini surfactant structure, all GPLs had a positive surface charge above $+30 \text{ mV}$. Generally, GPLs prepared with DOPE and DD 1:3 GPLs had similar zeta potential values (between $+40$ - 60 mV). Only in the cases of 12-3-12, 12-6-12

and 12-7NH-12, GPLs prepared with DOPE showed a higher zeta potential compared to GPLs made with DD 1:3. The effect of carbon spacer length on zeta potential showed a bimodal pattern (two peaks at approximately C3 and C10).

The shifts in zeta potential during NP assembly are summarized in Figure 3 E. Initially, the plasmid has a strong negative charge (-63 mV) and with the addition of gemini surfactants, the negative charge is neutralized. The low zeta potential ($\sim 0 - +25$ mV) indicates that these initial complexes are not stable and prone to aggregation. After the addition of the phospholipids, the zeta potential of NPs increased to $> +40$ mV stabilizing the initial GP complex formed between the gemini surfactant and DNA.

Morphology and structural studies

The morphological appearance of GP complexes was examined by AFM (Figure 4). The GP complexes formed from several gemini surfactants confirmed the heterogeneity of these particle populations (Figure 4A). The images show that in the absence of the phospholipid component each particle is made up of aggregated structures, each containing several compacted plasmids. The higher magnification images for the $m=12$ -series of gemini surfactants with increasing spacer length indicate more organized and spherical units at longer spacer lengths ($s=6$). The longer alkyl chain 16-3-16 surfactant forms more distinct multiunit complexes compared to the 12-3-12 surfactant, however the 16-3-16 GPs also have a population of small individual particles. Figure 4 B captures the temporal aspects of NP formation with the 12-3-12 and 16-3-16 surfactants. After about 15 minutes the GP complex formation was complete. The unique morphology of 12-3-12 GPs (spiders) versus 16-3-16 GPs (rosettes) was evident (Figure 4 A, B).

Upon addition of DOPE to 16-3-16 GPs, reorganization of NPs occurred and spherical particles formed (Figure 4C). Immediately following the addition of the respective gemini surfactant solutions to plasmids on mica surfaces, binding and compaction of plasmids was noticeable. The 16-3-16 GPs at a short (30s) incubation period showed greater morphological change and self-twisting compared to the 12-3-12 GPs which were still more loop-like in shapes, although the rough appearance confirmed the binding of 12-3-12 surfactants to the plasmids.

SAXS curves for each of the gemini surfactant compounds were obtained for GPLs prepared either with DOPE or with DD 1:3 (Figure 4D). The data indicate that the GPL particles organize into various polymorphic forms depending on the gemini surfactant chemical structure and the phospholipid component. DOPE, a neutral lipid, typically added to lipoplex formulations to assist with endosomal escape, in this case was used, also, as a helper lipid to mitigate the cytotoxicity of gemini surfactants. It has been shown that addition of cone-shaped DOPE may lead to formation of the inverse hexagonal phase (H_{II}^C) in lipoplexes.^{25, 26} GPL nanoparticles ($\rho_{+/-}$ 10:1) prepared with DOPE provided a main, sharp peak at q_{10} of about 0.1 \AA^{-1} (unit cell spacing (a) of about 70 \AA) for all gemini surfactants (Table 3), indicative of a 2D inverse hexagonal phase (q_{10} , q_{11} and q_{20}). The ratio of the first three Bragg peaks of the inverse hexagonal phase (1: $\sqrt{3}$:2: $\sqrt{7}$) is similar to the discrete cubic (Pm3n) phase (1: $\sqrt{3}$:2: $\sqrt{5}$), since we only had three peaks, the identification of the polymorphic phase is inconclusive. The GPL NPs prepared with DD 1:3 showed a broader peak most likely corresponding to lamellar morphologies (L_{α}^C) for all GPLs. The presence of lamellar structures in the NPs was also supported by TEM images (Fig 4 E). However, for

12-10-12 and 12-16-12 another weak scattering peak was present (q_{10}), indicative of an inverse hexagonal phase (Figure 4D; Table 4). In these latter two formulations, a mixture of lamellar and inverse hexagonal phase formed. In comparison with previously reported data on GP complexes²⁷, where we observed no long range order or specific polymorphic structure, the GPL systems shown here exhibit mixed polymorphic features. The calculated d-spacing for the single scattering peak of GP complexes showed inverse correlation with the head group areas of the m-s-m series of gemini surfactants²⁷.

Dye exclusion assay

Dye exclusion assays, using both PicoGreen and EtBr, were used to investigate the microenvironment around the nucleic acid cargo within the NP and to gain a deeper understanding of the role of NP composition in the self-assembly process. Dye exclusion occurs when cationic agents compact DNA resulting in an increase in DNA rigidity, thus denying the dye access to the DNA^{28, 29} and leading to a decrease in fluorescence intensity. GPs were capable of blocking approximately 95% of PicoGreen fluorescence as a result of a high degree of DNA-gemini surfactant association and compaction (Figure 5A). The gemini surfactant structure had a noticeable effect on dye blocking with GPs. Increasing spacer length in gemini surfactants from 3C (4.2±1.8%) up to 10C caused an increase of fluorescence (10.1±2.5%), followed by a significant drop for the 16C spacer (1.4±0.5%). Increasing the alkyl chain length of gemini surfactants did not affect dye blocking compared to 12-3-12 (16-3-16: 2.1±0.7%, 18-3-18: 2.9±1.2%). The GPs prepared from functionalized gemini surfactants 12-7NH-12 and Py-3-12 also did not provide a significant shift in the degree of dye blocking (4.3±1.3 and 3.9±1.8, respectively). The

addition of phospholipids normalized the degree of fluorescence exclusion among the final GPLs (Figure 5 B). Compared to GPs, where gemini surfactants determined the degree of dye blocking, the majority of the GPLs showed a similar degree of about 80% dye blocking. A significant shift was seen with GPLs prepared from gemini surfactants with longer carbon tails; 16-3-16 and 18-3-18 gemini surfactants produced a significantly higher extent (>95%) of fluorescence blocking. Furthermore, the phospholipids did not only normalize the GPs, but the composition also governed the final extent of dye blocking. It was observed that GPLs prepared from DD 1:3 had an overall higher blocking of fluorescence compared to DOPE counter-parts (Figure 5D).

The second dye exclusion assay with EtBr assay provided similar results to PicoGreen, such as the increased blocking of GPs relative to GPLs. However, in the case of Py-3-12, the two assays showed a significantly different result for both GP and GPL (Figure 5 C, D). In the PicoGreen assay, both GP and GPL prepared with Py-3-12 gemini surfactant was able to effectively block PicoGreen. However, with EtBr no fluorescence blocking was observed (Figure 5 C, D).

Cell viability

From our previous studies we have shown that free (unbound) gemini surfactant contributes to cytotoxicity^{30, 31}. To better understand the role of unbound gemini surfactants on cytotoxicity, the effect of GPs and GPLs on cell viability was evaluated in PAM212 keratinocyte culture (Figure 6). All GPs screened in this study showed cytotoxicity with cell viability generally lower than 20% (Figure 6A). An exception was with Py-3-12 GP which was significantly less cytotoxic (viability 57±7%). Whereas GPLs prepared with either DOPE or DD 1:3 did not significantly affect the health of

the PAM212 cells (greater than 95% viability) (Figure 6B).

Discussion

In this study we have characterized the assembly of gemini NPs using FCS and other complementary techniques. Gemini NPs are made in a two-step process, first by the addition of the gemini surfactant to the plasmid (the GP complex), followed by the addition of preformed phospholipid vesicles (GPL). The FCS study confirmed the formation of GP complexes and GPL NPs with defined size distribution determined from their diffusion coefficients which was strongly related to the structure of the respective gemini surfactant component (Table 1). In addition, data from the intensity histograms provided evidence that the initial complexation by gemini surfactants is not a simple compaction of a single plasmid, but a collection of multiple plasmids to form large GP complexes. The intensity histograms and scattergrams (Figure 2 iv) showed that both GPs and GPLs were composed of heterogeneous particle populations containing a different number of multiple plasmids. The GP population was more heterogeneous and contained upwards of 5-35 plasmids per complex, whereas the final GPLs were more homogeneous and contained between 2-20 plasmids per complex. The addition of phospholipids not only decreased the intensity of each peak, suggesting the presence of fewer plasmids per particle, it also increased the frequency of the peaks indicating the presence of more particles in solution (Figure 2). The morphology and internal structural organization of the GPs and GPLs were subsequently confirmed by AFM and TEM images and SAXS data.

The most important physicochemical properties of GPs and GPLs, such as diffusion coefficient, zeta potential and hydrodynamic diameter are seen to correlate well with the structure and properties of the respective gemini surfactants (Figure 7a). In the 12-s-12 series the diffusion coefficients and zeta potential of NPs correlate with the head group area of the gemini surfactants, whereas the particle size correlates with the CMC of the surfactants. The increase in diffusion coefficients of GPs and GPLs occurs up to $s=10$, in parallel with the head group area of the gemini. Since spacer length might be expected to increase head group area, it is surprising that above $s=10$ the area decreases. The rationalization of this behavior is that repulsion between the cationic centers of the head group for the shorter spacers ($s=3-8$) keep them somewhat fully extended but the spacer becomes more flexible and folding of the spacer into the hydrophobic alkyl region of the cation can occur leading to a smaller head group area^{32, 33, 34} and assuming a new conformation.³⁵ The packing arrangement between the gemini surfactant and plasmid in the GPs and GPLs would also be expected to be affected by this folding. The zeta potential results for the GPs and GPLs having gemini compound of different spacer length also illustrate a similar correlation.

For example GP 12-10-12 particles have the highest zeta potential ($\delta_{12-10-12}=+18.7$ mV) and smallest size (117.88 nm) compared to other gemini compounds. This higher surface charge could result in higher repulsion and therefore more stable particles that would resist aggregation. On the other hand, 12-3-12 with the smallest head group area produced GPs with very low surface charge ($\delta_{12-3-12}=+0.09$ mV) promoting aggregation and resulting in larger GP particles and a smaller diffusion coefficient. Another factor

influencing the size of GPLs is the critical micellar concentration (CMC) of the gemini surfactants. Significant shifts in the diffusion coefficient occurred with functionalized gemini surfactants. While their CMC is lower than their parent gemini surfactants (12-3-12 and 12-7-12) both Py-3-12 and 12-7NH-12 showed a significant increase in the magnitude of the diffusion coefficient (2.00 and $3.06 \times 10^{-12} \text{ m}^2/\text{s}$, respectively). In the case of Py-3-12, which has the lowest CMC of gemini surfactants screened, the GPs have the highest zeta potential and smallest size. This could be due to the ability of the pyrene functional group to intercalate with DNA providing additional stabilization.³⁶ The latter could also limit the formation of free gemini surfactant micelles and explain the observed decrease in cytotoxicity with Py-3-12 GPs compared to GPs. Further evidence of this intercalation is the ability of EtBr to penetrate Py-3-12 based gemini NPs, due to orientation of the pyrene tail into the DNA molecule. This could leave small areas exposed that would allow EtBr to enter as well.

Using the collective data sets for GP and GPL, a model of the assembly, involving supramolecular aggregates, of gemini NPs is proposed (Figure 7b). Based on gemini surfactant structure, the resulting GPs can be placed into three groups (Figure 7b - A, B, C) representing their specific physicochemical properties, such as zeta potential and the CMC of the gemini surfactant component. The first group includes the 12-s-12 series of gemini surfactants (Figure 7 A). Here the CMC is of medium magnitude providing sufficient number of monomer surfactants to neutralize the plasmids but leaving a low excess. This results in a low overall positive charge (zeta potential 0 - 5mV) and formation of many supramolecular aggregate GPs. The gemini surfactants with short spacers especially form GPs with very low zeta potential.

As spacer length increases (decreasing CMC), the zeta potential of GPs increase, which may be due to the difference in the interaction with the phosphate groups on the DNA⁴. The formulation also contains many free micelles (no plasmid) that may explain the cellular toxicity (20 % viability). The second group includes the py-3-12 gemini surfactant (Figure 7 B) with the lowest CMC (except for 12-16-12). Its binding to DNA is a combination of electrostatic and intercalation interactions, where the resulting GPs are more stable, generally having smaller particle size and higher zeta potential. Due to the relatively few unbound surfactants, the cellular toxicity is lower (60% viability). In the third group, the 12-7NH-12 gemini surfactant (Figure 7 C) has the highest CMC, with more available monomers and fewer free micelles to aid in the binding of gemini surfactants to plasmid, thus providing fewer large supramolecular complexes compared to the 12-series of surfactants. The resulting GPs are relatively stable, have small particle size and medium high zeta potential. Due to the relatively few unbound surfactant monomers and micelles the cellular toxicity is high (20% viability).

After the addition of phospholipids (Figure 7b, Step 2), mixed bilayers and potentially other polymorphic phases (hexagonal and/or cubic³⁷) are produced in the form of relatively spherical vesicle-like particles (GPL) with increased overall surface charge that stabilizes the individual GPLs. The number of plasmids within a GPL typically ranges between 2-20 plasmids per complex. In addition, some of the phospholipids also form plasmid-free mixed gemini-lipid vesicles.

Conclusions

In this study we have described the development and application of a novel method to

study gemini NPs using FCS. Monitoring of gemini NP assemblies was established using labeled plasmid and the optimal conditions for FCS measurement were determined. It was demonstrated that particle size of both the GPs and GPLs could be estimated by FCS and the values were validated by DSL and AFM. In addition to determining particle size, FCS was able to evaluate changes to the plasmid morphology during the various stages of assembly based on particle mobility in solution. When the FCS raw data was interpreted in an intensity-dependent manner, other values could also be determined such as an approximation of the number of plasmids within GP and GPL complexes. Overall, FCS provided insight into the mechanism of gemini NP assembly. Based on the findings, a model of gemini NP assembly has been proposed that gives prominence to the formation of GPs composed of "supramolecular aggregates" with size and aggregate number determined by the chemical structure of the gemini surfactants followed by stabilization due to the incorporation of the phospholipids to form the final GPLs.

Acknowledgements

The research in this paper was supported by operating and equipment grants from the Canadian Institutes of Health Research, the Natural Sciences and Engineering Research Council of Canada, the Canada Foundation for Innovation and the Ontario Research Fund. The generous support of the Canada Research Chairs Program is also gratefully acknowledged (M. Foldvari).

Portions of this research were carried out at the Stanford Synchrotron Radiation Lightsource (SSRL), a Directorate of SLAC National Accelerator Laboratory and an Office of Science User Facility operated for the U.S. Department of Energy Office of Science by Stanford University. The SSRL

Structural Molecular Biology Program is supported by the DOE Office of Biological and Environmental Research, and by the National Institutes of Health, National Institute of General Medical Sciences (including P41GM103393). The contents of this publication are solely the responsibility of the authors and do not necessarily represent the official views of NIGMS or NIH.

The authors would like to thank Jason Maley at the Saskatchewan Structural Sciences Centre, University of Saskatchewan, Saskatoon, SK, for the assistance with the Atomic Force Microscopic studies. We also thank Fred Pearson at the Canadian Centre for Electron Microscopy, McMaster University, Hamilton, ON, for assistance with the electron microscopic studies.

References

1. S. M. Moghimi, A. C. Hunter and J. C. Murray, *FASEB Journal*, 2005, **19**, 311-330.
2. S. Parveen, R. Misra and S. K. Sahoo, *Nanomedicine*, 2012, **8**, 147-166.
3. M. Donkuru, I. Badea, S. Wettig, R. Verrall, M. Elsbahy and M. Foldvari, *Nanomedicine (Lond)*, 2010, **5**, 1103-1127.
4. M. Donkuru, S. D. Wettig, R. E. Verrall, I. Badea and M. Foldvari, *Journal of Materials Chemistry*, 2012, **22**, 6232-6244.
5. I. Badea, C. Virtanen, R. E. Verrall, A. Rosenberg and M. Foldvari, *Gene Ther*, 2012, **19**, 978-987.
6. I. Badea, S. Wettig, R. Verrall and M. Foldvari, *Eur J Pharm Biopharm*, 2007, **65**, 414-422.
7. I. Badea, R. Verrall, M. Baca-Estrada, S. Tikoo, A. Rosenberg, P. Kumar and M. Foldvari, *J Gene Med*, 2005, **7**, 1200-1214.
8. P. Yang, J. Singh, S. Wettig, M. Foldvari, R. E. Verrall and I. Badea, *Eur J Pharm Biopharm*, 2010, **75**, 311-320.
9. I. Badea, R. Verrall, M. Baca-Estrada, S. Tikoo, A. Rosenberg, P. Kumar and M. Foldvari, *Journal of Gene Medicine*, 2005, **7**, 1200-1214.
10. I. Badea, S. Wettig, R. Verrall and M. Foldvari, *European Journal of Pharmaceutics and Biopharmaceutics*, 2007, **65**, 414-422.

11. J. Singh, P. Yang, D. Michel, R. E. Verrall, M. Foldvari and I. Badea, *Current Drug Delivery*, 2011, **8**, 299-306.
12. S. E. McNeil, A. Vangala, V. W. Bramwell, P. J. Hanson and Y. Perrie, *Current Drug Delivery*, 2010, **7**, 175-187.
13. N. K. Egilmez, Y. Iwanuma and R. B. Bankert, *Biochemical and Biophysical Research Communications*, 1996, **221**, 169-173.
14. I. Solodin, C. S. Brown, M. S. Bruno, C. Y. Chow, E. H. Jang, R. J. Debs and T. D. Heath, *Biochemistry*, 1995, **34**, 13537-13544.
15. B. Sternberg, K. Hong, W. Zheng and D. Papahadjopoulos, *Biochimica et Biophysica Acta - Biomembranes*, 1998, **1375**, 23-35.
16. K. Bacia and P. Schwille, *Methods Mol Biol*, 2007, **398**, 73-84.
17. K. Bacia, E. Haustein and P. Schwille, *Cold Spring Harbor protocols*, 2014, **2014**, pdb top081802.
18. E. Van Rompaey, Y. Engelborghs, N. Sanders, S. C. De Smedt and J. Demeester, *Pharmaceutical Research*, 2001, **18**, 928-936.
19. B. Lucas, K. Remaut, N. N. Sanders, K. Braeckmans, S. C. De Smedt and J. Demeester, *Journal of Controlled Release*, 2005, **103**, 435-450.
20. G. U. Nienhaus, P. Maffre and K. Nienhaus, *Methods Enzymol*, 2013, **519**, 115-137.
21. C. Wang, S. D. Wettig, M. Foldvari and R. E. Verrall, *Langmuir*, 2007, **23**, 8995-9001.
22. B. P. Binks, *Journal*, 1998.
23. I. M. Hafez and P. R. Cullis, *Advanced Drug Delivery Reviews*, 2001, **47**, 139-148.
24. A. S. Ulrich, *Bioscience Reports*, 2002, **22**, 129-150.
25. K. Ewert, N. L. Slack, A. Ahmad, H. M. Evans, A. J. Lin, C. E. Samuel and C. R. Safinya, *Current Medicinal Chemistry*, 2004, **11**, 133-149.
26. I. Koltover, T. Salditt, J. O. Rädler and C. R. Safinya, *Science*, 1998, **281**, 78-81.
27. M. Foldvari, I. Badea, S. Wettig, R. Verrall and M. Bagonluri, *J Exp Nanosci*, 2006, **1**, 165-176.
28. J. Olmsted Iii and D. R. Kearns, *Biochemistry*, 1977, **16**, 3647-3654.
29. C. M. Wiethoff, M. L. Gill, G. S. Koe, J. G. Koe and C. R. Middaugh, *Journal of Pharmaceutical Sciences*, 2003, **92**, 1272-1285.
30. L. Caillier, E. Taffin de Givenchy, R. Levy, Y. Vandenberghe, S. Geribaldi and F. Guittard, *Journal of Colloid and Interface Science*, 2009, **332**, 201-207.
31. A. Laatis, M. El Achouri, M. Rosa Infante and Y. Bensouda, *Microbiological Research*, 2008, **163**, 645-650.
32. S. D. Wettig and R. E. Verrall, *Journal of Colloid and Interface Science*, 2001, **235**, 310-316.
33. E. Alami, P. Beinert, P. Marie and R. Zana, *Langmuir*, 1993, **9**, 1465-1467.
34. F. M. Menger, J. S. Keiper, B. N. A. Mbadugha, K. L. Caran and L. S. Romsted, *Langmuir*, 2000, **16**, 9095-9098.
35. X. Chen, J. Wang, N. Shen, Y. Luo, L. Li, M. Liu and R. K. Thomas, *Langmuir*, 2002, **18**, 6222-6228.
36. A. Wolfe, G. H. Shimer Jr and T. Meehan, *Biochemistry*, 1987, **26**, 6392-6396.
37. M. Foldvari, S. Wettig, I. Badea, R. Verrall and M. Bagonluri, Boston, MA, 2006.
38. S. D. Wettig, P. Nowak and R. E. Verrall, *Langmuir*, 2002, **18**, 5354-5359.
39. S. D. Wettig, I. Badea, M. Donkuru, R. E. Verrall and M. Foldvari, *Journal of Gene Medicine*, 2007, **9**, 649-658.
40. P. Schwille, *Cell Biochemistry and Biophysics*, 2001, **34**, 383-408.
41. V. Bonasera, S. Alberti and A. Sacchetti, *BioTechniques*, 2007, **43**, 173-176.
42. S. H. Yuspa, P. Hawley-Nelson, B. Koehler and J. R. Stanley, *Cancer Research*, 1980, **40**, 4694-4703.
43. K. Bacia, S. A. Kim and P. Schwille, *Nature Methods*, 2006, **3**, 83-89.

Table 1 Diffusion coefficients of GPs and GPLs determined from FCS data.

A) Diffusion coefficients of various GPs from FCS measurements (n=4) and Particle size of GPs determined from FCS data using the Stokes-Einstein equation.

<i>Gemini compound</i>	<i>Mean diffusion coefficient ($10^{-12} \text{ m}^2/\text{s}$)</i>	<i>Mean diameter (nm)</i>	<i>CV (%)</i>
12-3-12	0.98	502.2	31.66
12-6-12	1.36	359.3	21.76
12-7-12	1.03	475.4	32.82
12-10-12	4.15	117.9	23.20
12-16-12	1.37	358.1	24.35
16-3-16	1.91	255.8	14.98
18-3-18	0.17	2837	175.6
12-7NH-12	3.06	159.9	8.65
Py-3-12	2.03	241.3	4.33

B) Diffusion coefficient of GPLs prepared with DOPE phospholipids. Particle size of GPLs prepared with DOPE phospholipids determined by FCS calculated using the Stokes-Einstein equation.

<i>Gemini compound</i>	<i>DOPE</i>			<i>DOPE:DPPC 1:3</i>		
	<i>Mean diffusion coefficient ($10^{-12} \text{ m}^2/\text{s}$)</i>	<i>Mean diameter (nm)</i>	<i>CV (%)</i>	<i>Mean diffusion coefficient ($10^{-12} \text{ m}^2/\text{s}$)</i>	<i>Mean diameter (nm)</i>	<i>CV (%)</i>
12-3-12	3.21	1525	19.11	3.11	157.5	13.18
12-6-12	3.24	151.4	15.25	3.21	152.5	19.46
12-7-12	2.64	185.5	13.90	3.76	130.4	6.32
12-10-12	4.60	106.5	6.40	3.84	127.5	13.56
12-16-12	3.06	160.1	15.71	3.47	141.1	28.15
16-3-16	2.85	172.1	12.66	3.68	133.2	17.34
18-3-18	0.58	849.7	66.68	2.36	207.2	79.62
12-7NH-12	3.92	124.9	6.17	4.33	113.1	8.38
Py-3-12	3.80	126.1	14.32	3.57	137.3	6.63

Table 2 Relevant physicochemical parameters of gemini surfactants, GPs and GPLs with interrelated properties. Critical micelle concentration (CMC); head group area of various gemini compounds were modified from Badea et al.⁹

<i>Gemini surfactant</i>	<i>CMC (mM)</i>	<i>(a^a) [nm²/molecule]</i>
<i>12-s-12</i>		
12-3-12	0.98	0.98
12-6-12	1.08	1.40
12-7-12	0.85	1.78*
12-10-12	0.62	2.16
12-16-12	0.12	1.44
<i>m-3-m</i>		
16-3-16	0.03	-
18-3-18	0.013	-
<i>m-NH-m</i>		
12-7NH-12	1.29	-
Pyrenyl		
Py-3-12	0.22	-

*12-8-12 is used to approximate 12-7-12 since data was not available. a^a = head group area

Table 3 Bragg peak positions and liquid crystal phase of GPL series consisting of plasmid, gemini surfactant and DOPE (see also Figure 4D).

Gemini surfactant		Bragg peak positions [\AA^{-1}]			Lyotropic liquid crystal	Unit cell spacing (a)* [\AA]
		1 st peak (q_{10})	2 nd peak (q_{11})	3 rd peak (q_{20})		
1	12-3-12	0.10094	0.17419	0.20119	H_{II}^c	71.88
2	12-6-12	0.10064	0.17149	0.20119	H_{II}^c	72.09
3	12-7-12	0.10064	0.17246	0.19914	H_{II}^c	72.09
4	12-10-12	0.10166	0.17349	–		71.36
5	12-16-12	0.10474	0.18272	–		69.27
6	16-3-16	0.10372	0.17451	–		69.95
7	18-3-18	0.10424	0.17817	–		69.58
8	12-7NH-12	0.10133	0.17361	0.20175	H_{II}^c	71.61
9	py-3-12	0.10084	0.17167	–		71.95

$$*a = \frac{2d}{\sqrt{3}}$$

Table 4 Bragg peak positions and liquid crystal phase of GPL series consisting of plasmid, gemini surfactant and DOPE:DPPC 1:3 (see also Figure 4D).

Gemini surfactant		Bragg peak positions [\AA^{-1}]		Lyotropic liquid crystal	Lamellar d -spacing or [\AA]	Unit cell spacing (a)* [\AA]
		1 st peak (q_{001})	2 nd peak (q_{10})			
1	12-3-12	0.08179	–	L_a^c	76.81	–
2	12-6-12	0.0815	–	L_a^c	77.09	–
3	12-7-12	0.08437	–	L_a^c	74.47	–
4	12-10-12	0.07785	0.09987	L_a^c, H_{II}^c	80.7	72.72
5	12-16-12	0.0762	0.09741	L_a^c, H_{II}^c	82.45	74.56
6	16-3-16	0.07649	–	L_a^c	82.13	–
7	18-3-18	0.07555	–	L_a^c	83.16	–
8	12-7NH-12	0.0802	–	L_a^c	78.34	–
9	py-3-12	0.08437	–	L_a^c	74.47	–

$$*a = \frac{2d}{\sqrt{3}}$$

Figure legends

Figure 1 Outline of FCS analysis and the general scheme of gemini NP assembly.

i) Instrumental set-up of the FCS system using a confocal microscope: Laser excitation enters the object from behind and is focused on the sample. Emission from the sample is collected through the objective and is separated from the excitation via a dichroic mirror. Emission is then focused in front of a pinhole placed in front of the APD to remove out-of-focus fluorescence. This provides FCS the ability to monitor a focal volume of less than one femtoliter. (B) Principle of FCS measurements: fluorescence fluctuations are recorded by the APD as the fluorophores diffuse through the focal volume. The temporal recording is subjected to the autocorrelation function and generates a correlation curve ($G(\tau)$) which is used to reveal parameters of about the fluorophore⁴³.

ii) General chemical structure of gemini surfactants. Gemini surfactants are composed of two hydrophobic tails and two positively charged quaternary ammonium head groups linked by a spacer (A). Gemini surfactant structural modifications for this study include changes to spacer length (B), tail length (C) and addition of various functional groups such as an imino group in the spacer and a pyrene group in the alkyl tail (D).

iii) Schematic diagram of gemini NP assembly. Plasmids are pre-compacted by the addition of dicationic gemini surfactants to form GP. The GPs is then rearranged through the addition of the helper lipid vesicles to form the completed gemini NP (or GPL).

Figure 2 FCS analysis of GP and GPL particles.

i) Raw intensity count rates for gemini nanoparticle assembly. Count rate measurements for Cy5-plasmid (A), 12-3-12 GP (B) and 12-3-12 GPL (C); (10 seconds of the 250 second measurements are shown). Intensity histograms for Cy5-plasmid (D), 12-3-12 GP (E) and 12-3-12 GPL (F).

ii) FCS measurement of GPLs at $\rho_{+/-}$ 10:1 with 12-3-12 and DD 1:3 phospholipid. Open triangles shows the ACF and red line represent the fitting model for the ACF for GPL. Cy5-plasmid GFP (solid line), GP (dashed line) are added as references. DNA concentration for all samples was 2 ng/ μ L. A) Original ACF B) Normalized ACF.

iii) ACF of GPs (panel I) and GPLs (panel II) prepared with various gemini surfactants. Effect of gemini spacer length (A); alkyl tail length (B); and i functionalization (C).

iv) Estimation of number of plasmids per GP and GPL particles based on average individual counts per particle (kHz) divided by average individual counts of plasmid (200 kHz) n=50-80 runs. Median plasmid number per particle: 12-3-12 GP = 6.7; py-3-12 GP = 8.4; 12-7NH-12 GP = 8.1 and 12-3-12 GPL_{DOPE} = 6.0; py-3-12 GPL_{DOPE} = 6.9; 12-7NH-12 GPL_{DOPE} = 5.9; 12-3-12 GPL_{DD} = 5.9; py-3-12 GPL_{DD} = 1.3; 12-7NH-12 GPL_{DD} = 6.9.

Figure 3 Particle size measurements of GPLs by DLS. Zeta-average particle diameter (A) and polydispersity index (B) of GPLs prepared with a series of gemini surfactants and neutral phospholipids DOPE or DD 1:3. Values are expressed as mean \pm SD, n=4.

Zeta potential measured at different stages of gemini NPs assembly. Effect of gemini surfactant structure on zeta potential of GPs (C) and GPLs prepared with DOPE and DD 1:3 phospholipids (D). Values expressed as mean \pm SD (n=4). pH of DOPE and DD 1:3 GPLs was between 6.5-7.1. Cluster plot of zeta potential of free plasmid, GPs and GPLs (E).

Figure 4 Morphological and structural evaluation of GPs and GPLs. Atomic force microscopy of GP complexes (four different examples are shown with 12-3-12, 12-4-12, 12-6-12 and 16-3-16) (A) and the NP in-process assembly images for 12-3-12 and 16-3-16 GPL (B, C). D) SAXS profiles of a series of GPL prepared with DOPE and GPL prepared with DD 1:3; Curve 1: 12-3-12; 2:12-6-12; 3:12-7-12; 4:12-10-12; 5:12-16-12; 6:16-3-16; 7:18-3-18; 8:12-7NH-12; 9:py-3-12; E) Transmission electron microscopic images of GPL DD:1:3 particles a) 12-3-12; b); py-3-12 c) 12-7NH-12.

Figure 5 PicoGreen (A, B) and ethidium bromide (C, D) dye exclusion assay for various GP (A and C) and GPLs (B and D), reported as percentage of fluorescence remaining relative to free plasmid. Values expressed as mean \pm SD (n=4).

Figure 6 Cell viability assay using Presto Blue reagent in PAM 212 keratinocytes.

Cell viability after treatment with various GPs (A) and GPLs (B). Values expressed as mean \pm SD (n=4).

Figure 7 Relationship between physicochemical parameters of gemini surfactants, GP and GPL and a model for NP assembly.

a) Correlation between gemini surfactant spacer length, physicochemical attributes and measured parameters modeled by third order polynomial (cubic) fitting

b) Diagram of the proposed supramolecular aggregate model of gemini NP assembly.

Step 1: Free negatively charged plasmids are initially condensed by the binding of dicationic gemini surfactant molecules. The initial compaction produces gemini-plasmid units that aggregate due to the neutralization of surface charge and decreased repulsive forces and form the supramolecular GPs which have differing properties depending on the structure and physicochemical properties of the gemini surfactant involved.

A) In case of the m-s-m gemini surfactants which have the relatively high CMC among the gemini surfactants used, providing sufficient number of monomers, that result in GP complexes with low zeta potential (0 - +5 mV; except for very long spacers s=10 and 16, +16-18 mV). Since CMC decreases with increasing spacer length (12-series), this is consistent with the measured zeta potential of GPs. The formulation also contains many free micelles (no plasmid) which contribute to cellular toxicity.

B) The pyrene gemini surfactant with the very low CMC, in addition to electrostatic binding to plasmid can also bind by intercalation which results in a more stable GP with the highest zeta

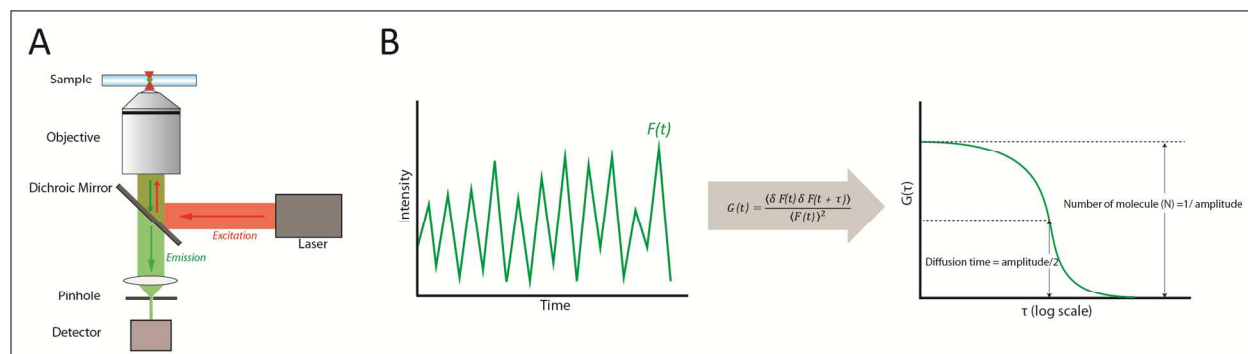
potential (+25 mV) and smallest particle size. Due to the relatively few unbound surfactant the cellular toxicity is lower (60% viability).

C) The spacer functionalized 12-7NH-12 gemini surfactant has the highest CMC producing GPs with intermediate zeta potential (+10 mV). The presence of extra unbound monomers and micelles contribute to cellular toxicity.

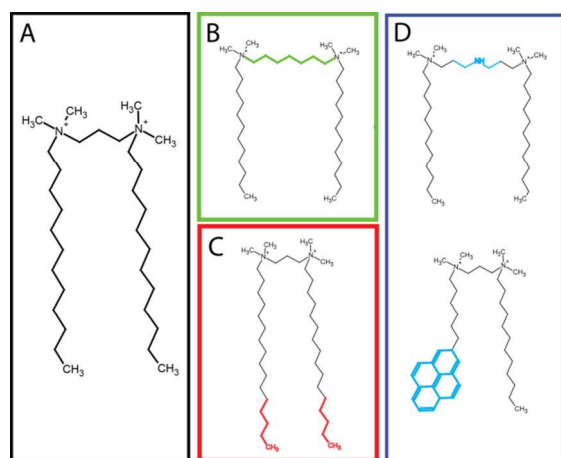
Step 2: The added phospholipids form mixed bilayers and potentially other polymorphic phases (hexagonal and cubic ³⁷) with the gemini surfactants and produce a relatively spherical vesicle-like particles (GPL) with increased overall surface charge which stabilizes the individual GPLs. In addition, some of the phospholipids may also form plasmid-free mixed gemini-lipid vesicles.

Figure 1

i)



ii)



iii)

Gemini nanoparticle assembly

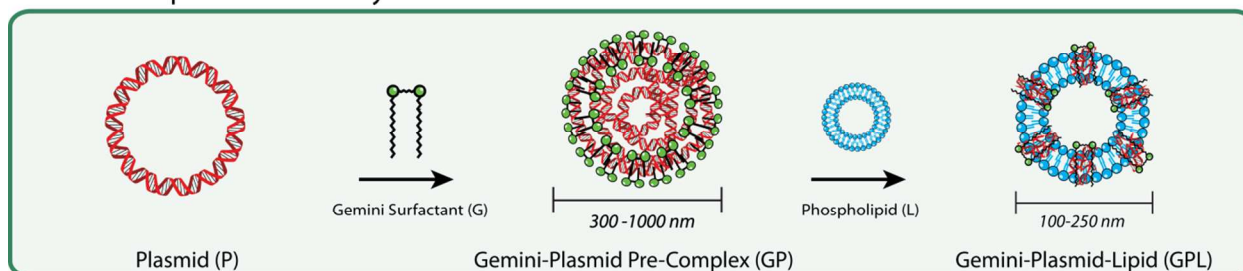
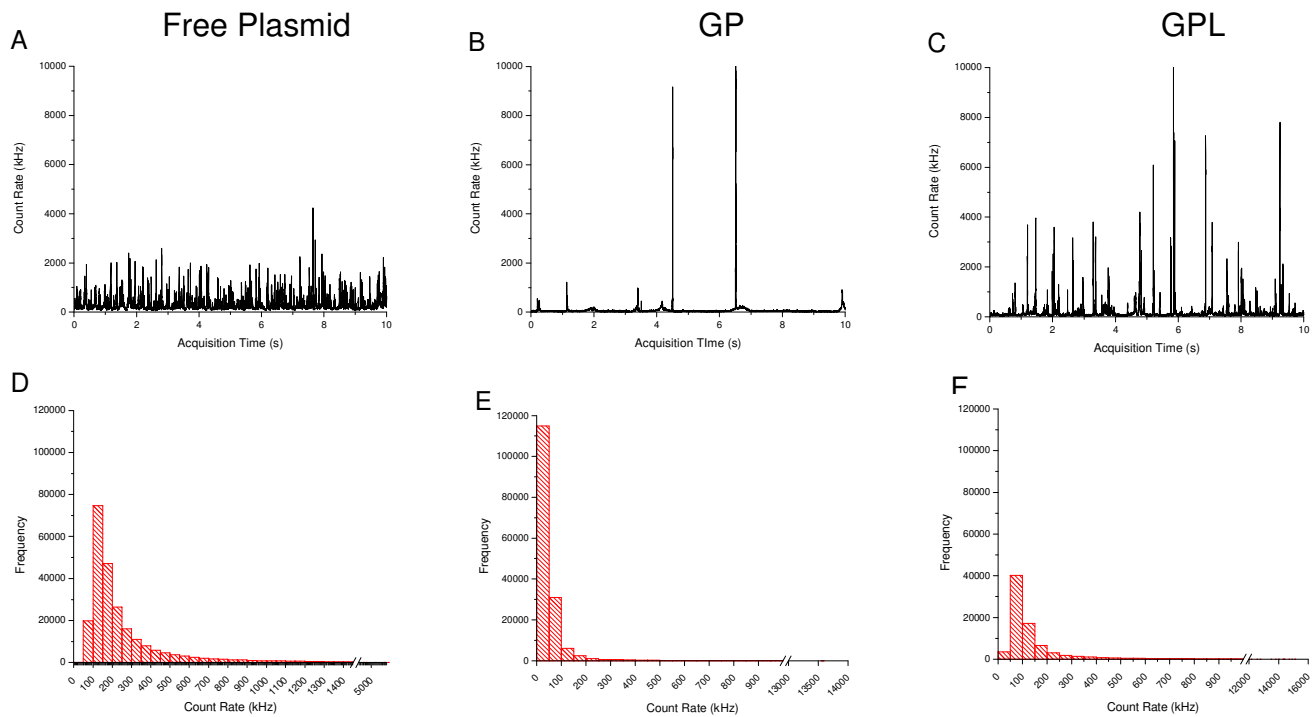
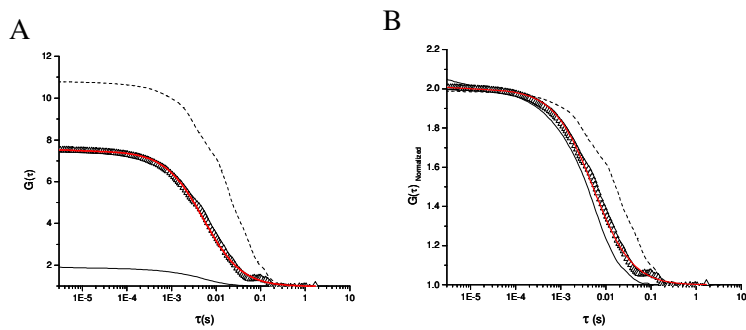


Figure 2

i)

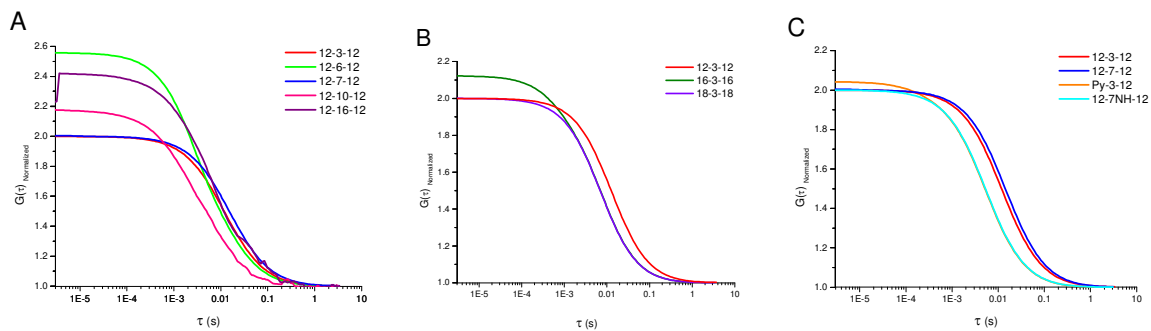


ii)

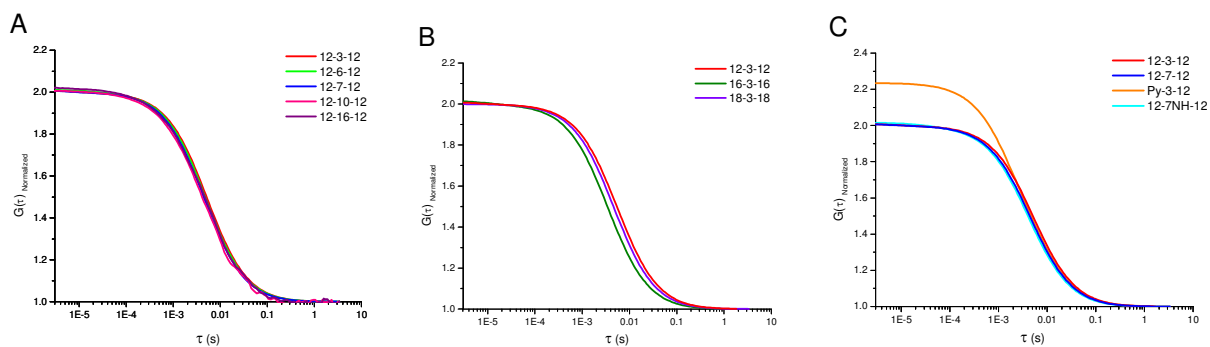


iii)

Panel I: GP



Panel II: GPL



iv)

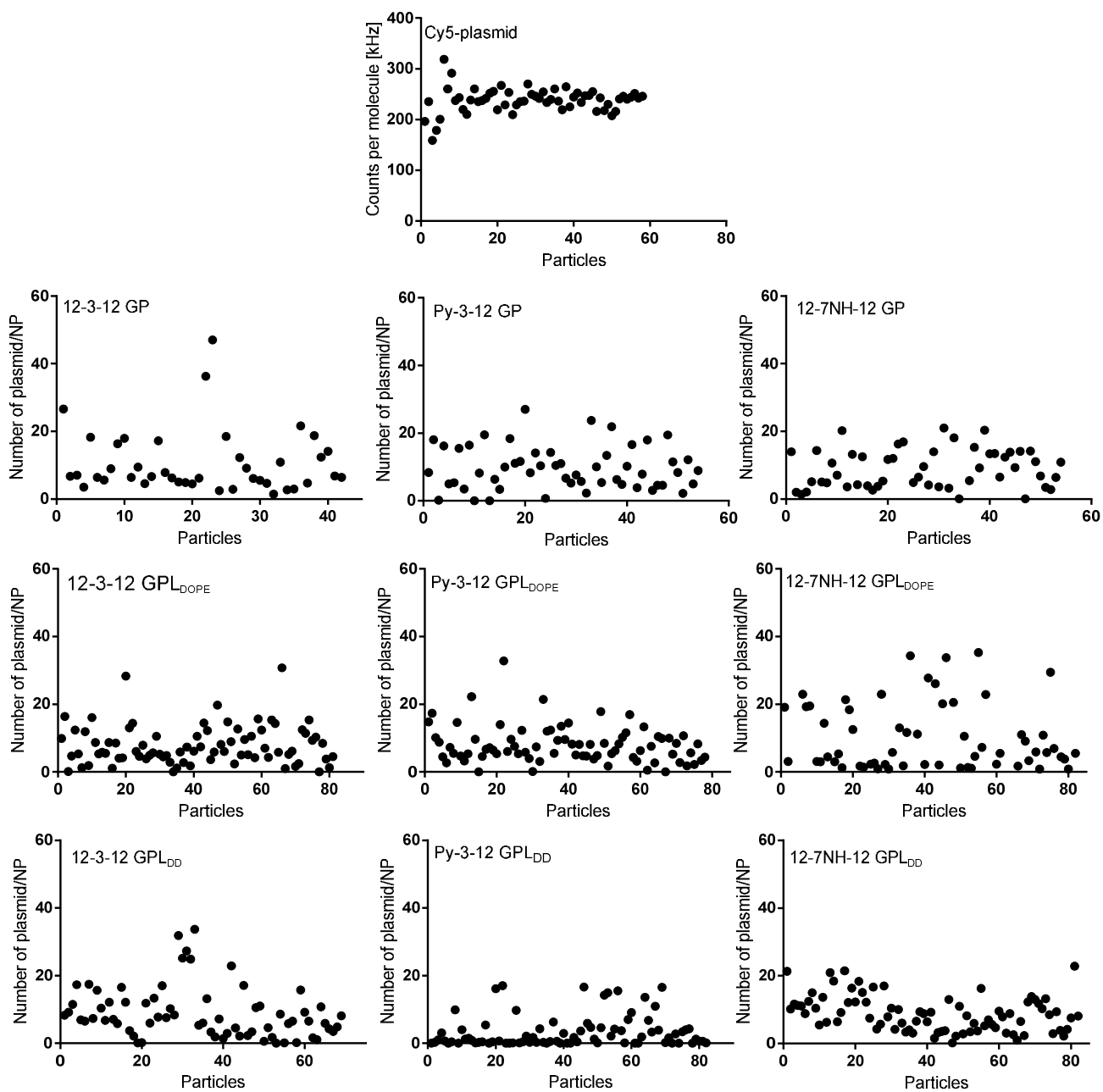


Figure 3

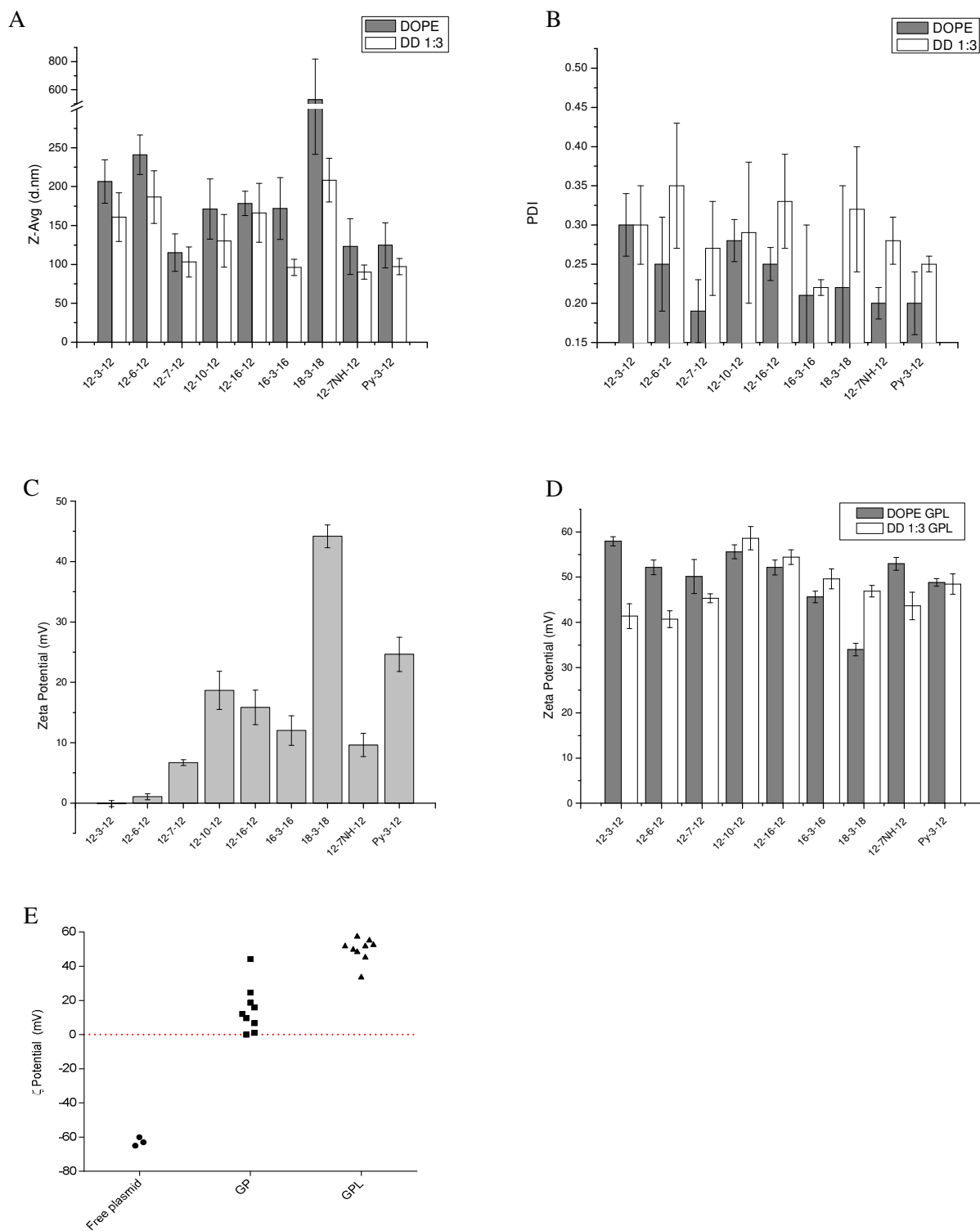


Figure 4

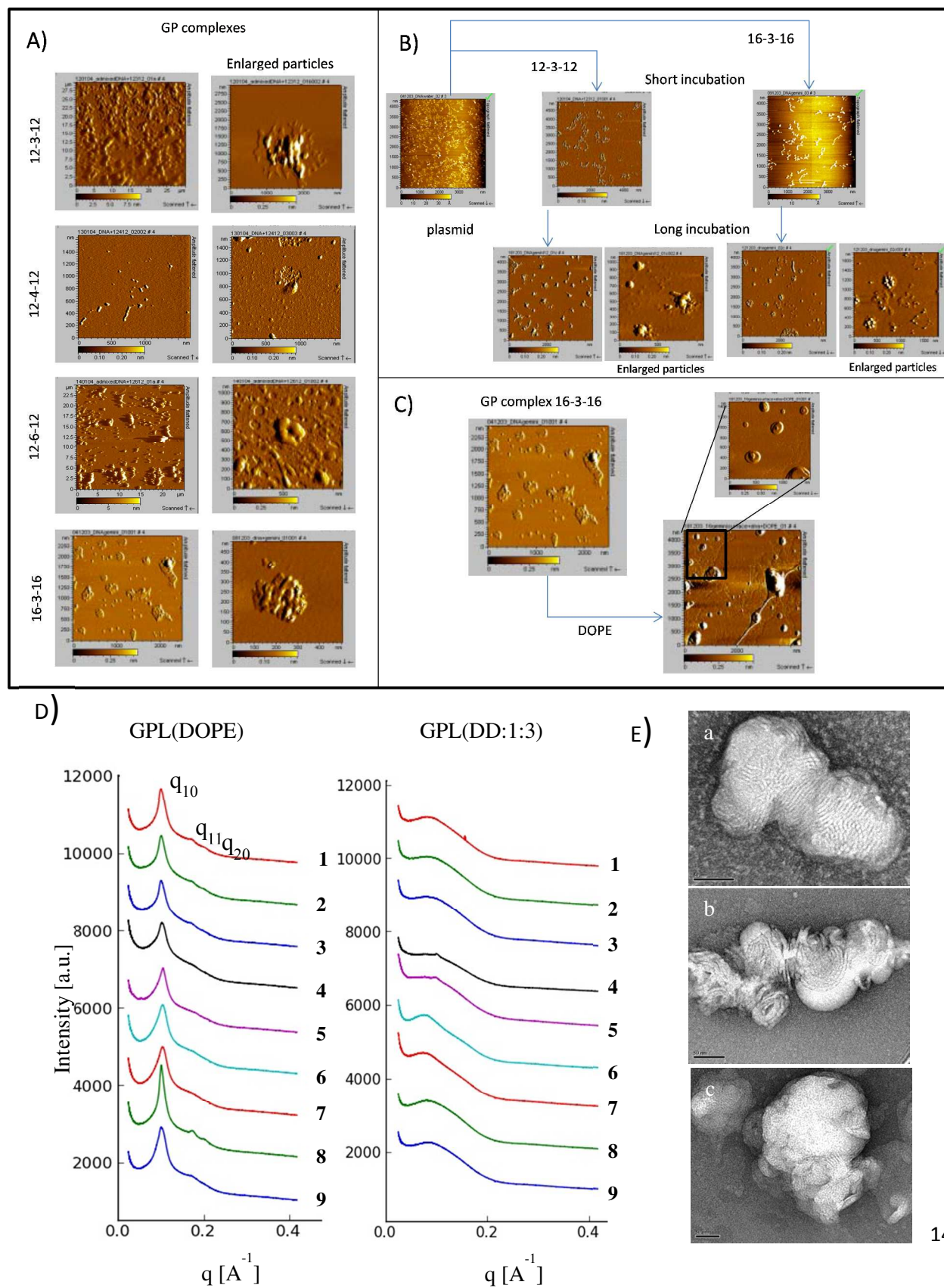


Figure 5

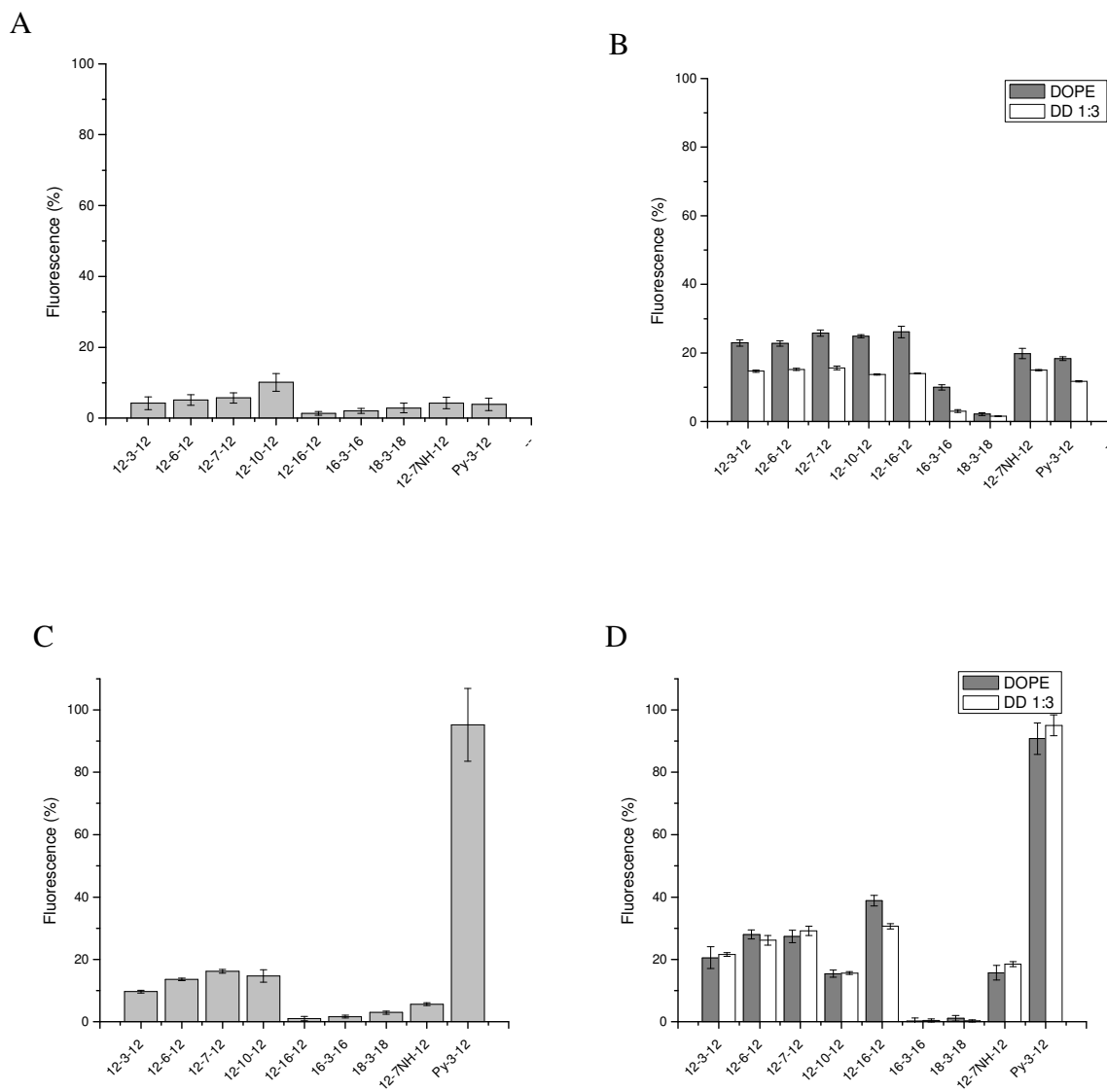
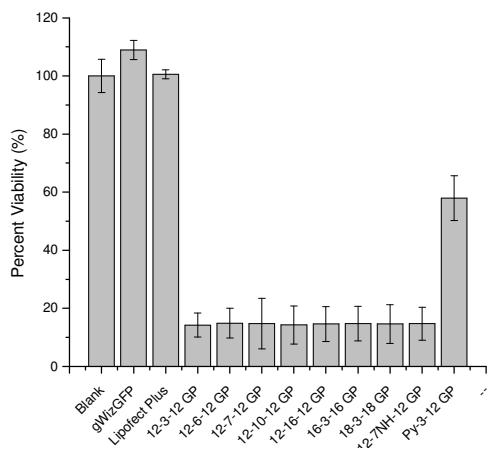


Figure 6

A



B

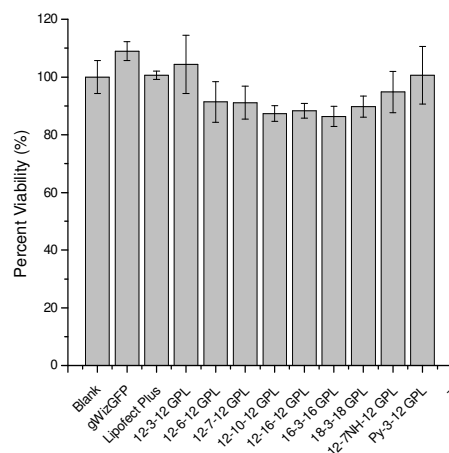
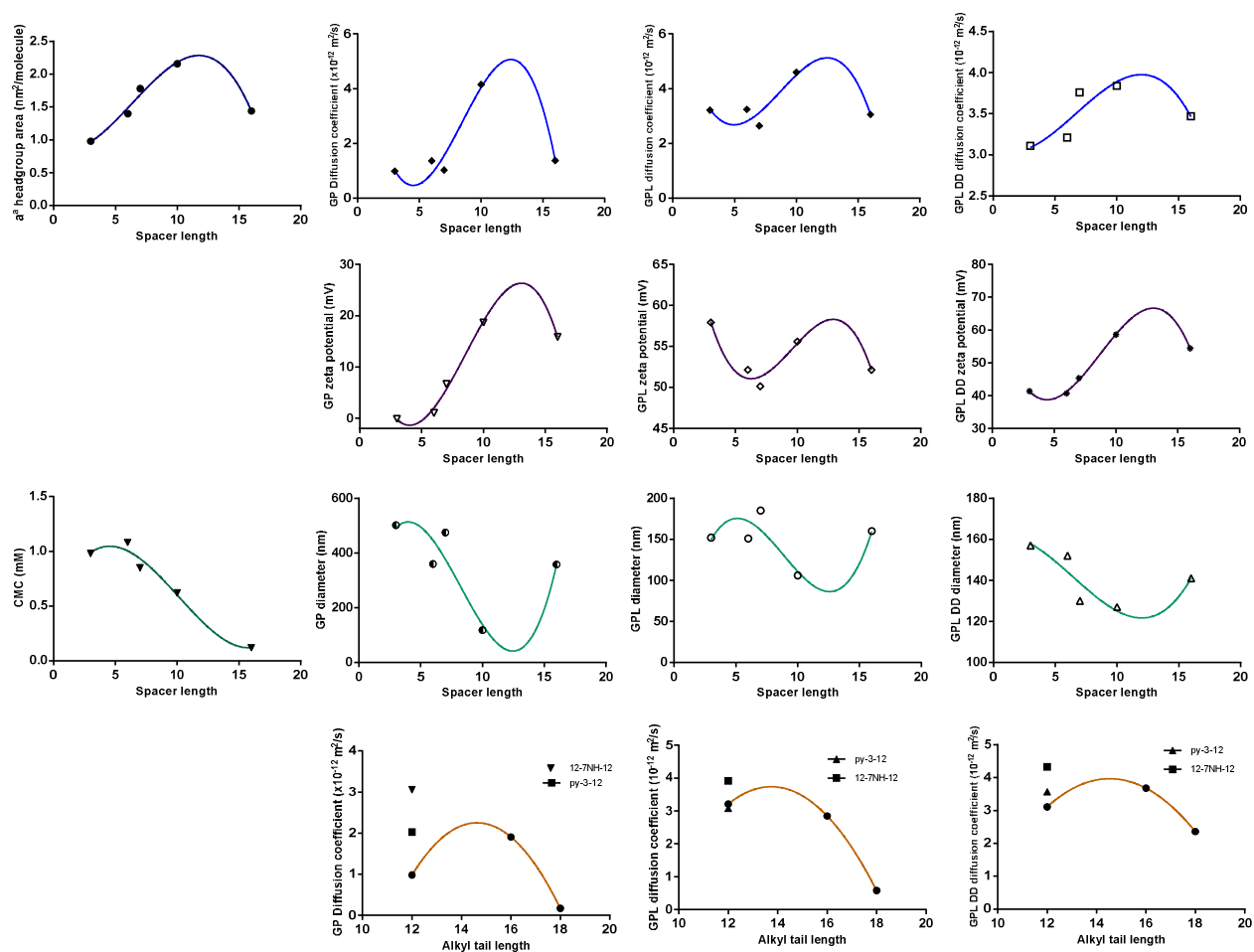


Figure 7

a) Correlation between gemini surfactant spacer length, physicochemical attributes and measured parameters modeled by third order polynomial (cubic) fitting



b) Diagram of the proposed supramolecular aggregate model of gemini NP assembly.

